AIAA JOURNAL
Vol. 43, No. 6, June 2005

Compensation of Anelastic Error in Force Measurement

Boris A. Slutsky*
NASA Ames Research Center, Moffett Field, California 94035

The output of a force sensor can change over time under constant load as a result of anelastic creep of components. An empirical model of this behavior in force sensors is presented. Unlike previous work, the model does not a priori assume an exponential functional form for the creep. Once parameters are obtained in a simple calibration procedure, sensor output can be quantitatively predicted, and the error that would otherwise appear in the measurement can be corrected mathematically. The proposed model captures over 98% of anelastic behavior in the bending beam load cell studied and is expected to apply to other force sensors as well, including wind-tunnel strain-gauge balances. The model also helps visualize the consequences of anelastic creep in typical calibration and test scenarios. Results demonstrate that creep-induced error can reach or even exceed 0.3% of measured load, depending on the quality of the sensor and the load schedule. Examples are given of loading patterns susceptible to the error.

I. Introduction

THE measurement of mechanical forces and moments plays an important role in aerodynamic testing. Measurement uncertainty of less than 0.1% full scale is often sought.[1] A variety of sensing devices are available, from inexpensive bending beam load cells to six-component wind-tunnel balances. In most if not all cases, forces and moments are deduced from the amount of strain in a spring element, such as a beam or an elastic membrane. The strain, in turn, is revealed by a strain gauge, typically an electrically resistive film on thin plastic backing, bonded to the spring. Nonlinearity, hysteresis, memory, and other aberrations in the stress-strain characteristic of the material, as well as defects of the adhesive and the gauge, if not accounted for, directly contribute to instrument error.

This paper reports on an investigation of anelastic effects as a factor in force measurement. As described in more detail in the following, anelasticity manifests itself in metals by gradual increase of strain under constant stress over time periods on the order of minutes, hours, and even weeks. The resultant change in sensor output can be mitigated by the use of strain gauges with a tendency to creep in the opposite direction and can in principle be reduced to 0.03–0.05% of applied load, which is the tolerance limit for National Type Evaluation Program (NTEP) certification.[2] However, many practical instruments perform less well. Net output drift ranging from −0.49% to +0.76% has been observed in new wind-tunnel balances,[3] and the bending beam load cells studied in the present work exhibited drift of +0.4% to +0.7%. The impact of anelasticity on the measurement varies with calibration and test procedures employed. Section IV demonstrates through simulation that errors up to 0.3–0.4% or greater may result, enough to compromise, for example, experiments performed at NASA Ames Research Center to quantify small changes of rotor thrust caused by a nearby second rotor. The error is systematic and escapes detection by analytic procedures currently in use because it is readily absorbed into the linear term of the mathematical model.

In metals, the phenomenon of continuing deformation under constant load (Fig. 1) is well known. The additional strain acquired over time might be permanent (plastic) or recoverable after the load is removed (anelastic).[4] Permanent strain dominates under stresses close to the yield point, or at elevated temperatures, but in some cases even under stresses 50% below yield at room temperature.[5] (The high-temperature condition is of importance to the design of gas turbine blades, where deformation ultimately limits the components' working life.) Plastic creep generally advances through so-called primary, secondary, and tertiary phases, characterized respectively by decreasing, constant, and rapidly increasing strain rate leading to fracture. At low temperatures, however, plastic strain grows logarithmically with time,[6] a law first reported by Philips (1905) for various metals and some nonmetallic materials.

Only anelastic (recoverable) creep is present in force-sensing instruments because their operating regime is always chosen to avoid any permanent effects. Zener[7] credits to Weber (1834) the first observations of anelastic strain in metals, and to Boltzmann (1876) the insight that it obeys the principle of linear superposition. This being the case, strain ε has a well-defined step response function $u(t)$ with respect to stress σ, such that

$$\varepsilon(t) = \int_0^\infty u(\tau)\dot{\sigma}(t-\tau)\,\mathrm{d}\tau \tag{1}$$

in the time domain, and also has a well-defined spectral response $E(\omega)$ in the frequency domain. The two descriptions are related by the Laplace transform ℓ: $E(\omega) = (s\ell\{u\})|_{s=j\omega}$. The quantity $\tan\delta = \tan\{\arg[\mathrm{E}(\omega)]\}$, also frequently denoted $Q^{-1}(\omega)$, is referred to as internal friction, and its variation with frequency as internal friction spectrum.

The pioneering works on anelastic theory are due to Zener[7] and Lubahn.[4] Zener introduces the subject with the first-order differential relation of a so-called standard linear solid:

$$\sigma + \tau_\varepsilon\dot{\sigma} = M_R(\varepsilon + \tau_\sigma\dot{\varepsilon}) \tag{2}$$

In a material described by Eq. (2), part of the strain complies instantaneously with stress, and the remainder is added over time, in full agreement with Fig. 1. The corresponding step and frequency responses are found by solving Eq. (2) for ε with the appropriate stress stimuli σ,

$$u(t) = M_R^{-1}\left[1 + \left(\frac{\tau_\varepsilon}{\tau_\sigma} - 1\right)e^{-t/\tau_\sigma}\right] \qquad (t \geq 0) \tag{3a}$$

$$E(\omega) = M_R^{-1}\frac{1 + j\omega\tau_\varepsilon}{1 + j\omega\tau_\sigma}, \qquad Q^{-1} = \tan\delta = \frac{\omega(\tau_\sigma - \tau_\varepsilon)}{1 + \omega^2\tau_\sigma\tau_\varepsilon} \tag{3b}$$

The characteristic form taken by the spectrum $Q^{-1}(\omega)$ in Eq. (3b) crests at $\omega = \omega_0 = (\tau_\sigma\tau_\varepsilon)^{-1/2}$. From the magnitude $Q_0^{-1} = \frac{1}{2}(\tau_\sigma\tau_\varepsilon)^{-1/2}(\tau_\sigma - \tau_\varepsilon)$ of the peak and its location ω_0, the time parameters τ_σ, τ_ε are readily recovered,

$$\tau_\varepsilon/\tau_\sigma = 1 + 2Q_0^{-2} - 2Q_0^{-1} \Rightarrow u(t) \approx M_R^{-1}\left[1 - 2Q_0^{-1}e^{-\omega_0 t}\right] \tag{4}$$

Received 24 August 2004; revision received 7 December 2004; accepted for publication 8 December 2004.

*Ames Associate, Aeromechanics Branch, Army/NASA Rotorcraft Division, M/S N246-012; bslutsky@mail.arc.nasa.gov.

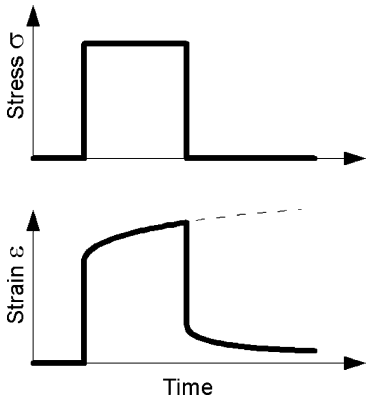

Fig. 1 Anelastic stress-strain relationship. Step response of strain to stress is shown by dashed line.

where the approximation holds when (as tends to be the case) $Q_0^{-1} \ll 1$.

The formalism of Eq. (2) is appealing because theoretical motivation exists for it in micromechanical and thermodynamic models of grain boundary relaxation in a polycrystalline solid. Thermodynamic considerations also suggest that process times τ_σ, τ_ε scale with temperature T by the Arrhenius factor

$$\tau \sim \exp(H/RT) \tag{5}$$

where $R = 8.31 \cdot \mathrm{J \cdot mole^{-1} \cdot K^{-1}}$ is the universal gas constant and H is the activation energy. Internal friction Q^{-1} therefore exhibits a distinct peak both as a function of frequency ω at constant temperature and as a function of temperature with ω held constant. It is in this latter manner that relaxation peaks were first observed in polycrystalline aluminum.[8] The most pronounced spectral line ($Q_0^{-1} = 0.08$) occurs there at $T = 290^\circ$C with $\omega_0 = (\tau_\sigma \tau_\varepsilon)^{-1/2} = 2\pi$ s^{-1} and $H = 1.4 \times 10^5$ J · mole^{-1} (Ref. 9), equivalent via Eq. (5) to $(\tau_\sigma \tau_\varepsilon)^{1/2} \sim 10^{11}$ s (4000 years) at $T = 20^\circ$C, and consequently cannot account for room temperature phenomena. In any event, the line disappears below $T = 130^\circ$C (Ref. 9). Other peaks, including some at room or near-room temperature [e.g., S-peak in α-Fe, $T = 41^\circ$C, $\omega_0 = 2\pi$ s^{-1}, $Q_0^{-1} = 0.003$ (Ref. 10)], were subsequently discovered and linked to relaxation of various crystalline defects or diffusion of interstitial atoms (e.g., carbon atoms in steel). The spectrum of pure single-crystal aluminum exhibits no sharp features.[9]

But although the maxima of the internal friction spectrum have been seen and quantified by many researchers, identification of the exponential decay terms, Eq. (3a), in the creep function $u(t)$ proved problematic. The difficulty lies not in the failure of linear superposition, Eq. (1), but in the effect of spectral background on time-domain behavior. The superposition has been amply demonstrated by the comprehensive work of Lubahn,[4] and the approximate relation between internal friction and creep derived by Zener from the Laplace transform identity $E(\omega) = (s\ell\{u\})|_{s=j\omega}$ has also been experimentally confirmed.[8] Yet, for example, the data obtained by Lubahn[4] from 0.5-in. (12.7-mm) steel rods at 800°F (476°C) could not be represented with fewer than four exponential modes, having widely different time constants and no obvious physical interpretation. More recently (and with vastly superior computing technology at their disposal), Sgobba et al.[11,12] sought a similar decomposition of the step response $u(t)$ measured at room temperature in thin flexing strips of aluminum and copper. The reduction was found to be unstable and produced no result that could be credibly related to the internal friction spectra of the materials involved. Lubahn[4] and Sgobba et al.[11,13] both note that the anelastic strain shows no tendency toward saturation, even in tests extending over 20 days (10^6 s).

Neither Lubahn nor Sgobba et al. introduce anelastic theory into the context of force-sensing instrumentation. The only works, to this author's knowledge, that do so are those of Steinle[1] and Steinle et al.[14] Steinle et al. compared two calibrations of the NASA Langley 104B balance. Both calibrations followed the same 408-point schedule representative of a load sequence in a wind-tunnel test, but in one case the loads were applied at a slower rate of one every 14.49 s on average, instead of the normal average rate of one load every 5.85 s. The discrepancy between the two calibrations was attributed to anelastic behavior. Elements of the 104B balance were modeled with the standard linear solid equation (2), in which, however, the time constants were permitted to vary with strain and strain rate:

$$\tau_\sigma = k_{01} + k_1 \varepsilon,$$

$$\tau_\varepsilon = \tau_\sigma + k_{00} + k_2 \varepsilon + k_3 \varepsilon^2 + k_4 \varepsilon \frac{\partial \varepsilon}{\partial t} + k_5 \frac{\partial \varepsilon}{\partial t} + k_6 \varepsilon^2 \frac{\partial \varepsilon}{\partial t} \tag{6}$$

The strain ε and the strain rate $\partial\varepsilon/\partial t$ in Eq. (6) were known at each data point (the latter approximately, because individual points were not time stamped). The constants $k_2, \ldots, k_6$ were treated as independent for tension and compression, and k_{00}, k_{01}, k_1 were treated as independent for tension increase, tension decrease, compression increase, and compression decrease. It was also necessary to include the residual anelastic strain existing prior to the test. The equations were regressed to find these 23 unknown parameters. When applied to the same data set that was used for regression, the model explained 77% of the difference between fast and slow calibrations of the axial force gauge.[1]

The objective of the present work, as in Refs. 1 and 14, is to propose a method for compensating anelastic effects at the data-reduction stage. However, the approach herein is based not on the standard linear solid theory, Eqs. (2) and (3a), but (following Lubahn[4]) on the superposition principle, Eq. (1). Experiments were designed to directly acquire the step response $u(t)$ of a given load cell over time periods of 20 min to 1 h (1200–3600 s). Section II describes the equipment and procedures employed. The data are found to be effectively extrapolated by a logarithmic function of time. The logarithmic form is entirely phenomenological, but with only two free parameters it explains over 98% of time-varying behavior, in both back- and cross-calculation, of the load cell for which it was estimated. More importantly, bridge outputs, including the contributions from the adhesive and strain gauge creep, are found to obey the linear superposition law that Eq. (1) expresses for strain. When used to correct a calibration data set, the linear superposition model reduced the uncertainty of the sensitivity parameter from 0.4% to 0.1%, and rms residual error from 0.08% to 0.02% of gauge capacity. Section III reports the results obtained with bending beam load cells of two different types. Section IV employs computer simulation to illustrate the consequences of anelasticity in typical calibration and test scenarios. A systematic error on the order of 0.3% is predicted, such that it would go undetected in conventional data reduction. Section IV also reviews evidence of anelasticity in wind-tunnel strain gauge balances. Despite extensive use of balances in aerodynamic testing, their anelastic properties have thus far drawn little attention. The only direct empirical data available are from Cahill et al.[3]; they suggest that although most balances exhibit lower creep than the inexpensive load cells used in Sec. III, some perform as poorly or even worse. At the end of Sec. IV, the role of adhesive and gauge creep is briefly discussed. Conclusions are summarized in Sec. V.

II. Experimental Methods

Figure 2a sketches the experimental arrangement with which most of the data in this paper were obtained. A commercially available Futek model L1501 bending beam load cell is mounted in horizontal cantilever position, and an extension bar is connected to its free end. Weights are placed on a tray suspended at the far end of the bar; this operation is manual, but normally takes less than 2 s and is treated as step loading in the analysis. Because the stand is also intended for microrotorcraft work, a small electric motor, gears, and a propeller are attached to the extension bar. These components play no role in the experiment, except as tare weight ensuring that stress direction is not reversed. A micrometer screw situated under the load cell can be used to support it against accidental overload. The screw is withdrawn prior to any measurement.

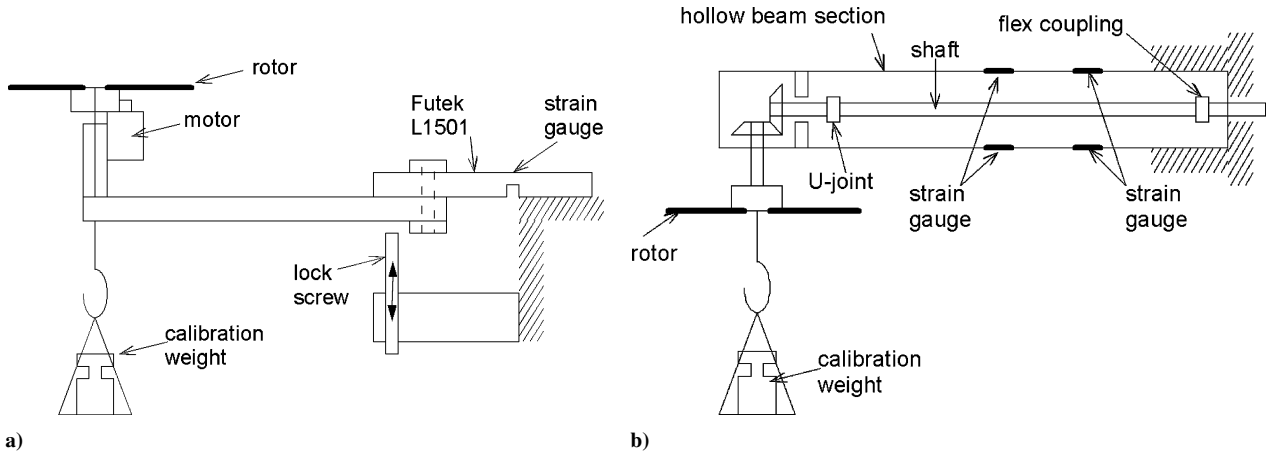

Fig. 2 Experimental setup with a) Futek L1501 load cell and b) Micro-Measurements EA-13-250PD-350 full bridge strain gauges.

The L1501 load cell is a $0.28 \times 0.18 \times 2.56$ in. ($7.1 \times 4.6 \times 65$ mm) long section of 17-4PH stainless steel with an integral thin (0.062 in.; 1.57 mm) flex membrane to which a strain gauge is bonded on one side. Electrically, the gauge is a 1000Ω resistive bridge, such that an excitation voltage is applied across two of its nodes and the signal voltage is measured across the other two. A Sorensen DCS-40-25 power supply provided the nominal 12-V excitation. Measured signal was always divided by the measured excitation, even though the latter proved to be quite stable (rms noise 1 part in 10^5, overnight excursion three parts in 10^4). Full-scale output of the gauge is 1 mV/V for a 5-in. lbf (0.565-Nm) load. The dead weight of microrotor hardware preloads the cell to 0.3 of full scale; a 200-g weight at the tray represents 0.5 of full scale. The 5-in. lbf full-scale load is estimated from the geometry of the element to produce 28-ksi (190-MPa) outer fiber stress (and hence 10^{-3} outer fiber strain) in the flex membrane. Yield strength of commercially available 17-4PH steel is nominally 1000 MPa. The amount of bending under full load was not recorded; Futek specifies 0.4 deg.

The signal voltage (4–10 mV) was measured with an HP34970A switching multimeter. Listed basic dc accuracy of the meter, under the conditions used, is 0.004 mV + 0.0005 mV/°C. Ambient temperature varied by less than 0.3°C in most experiments. Voltmeter error therefore would not exceed 4×10^{-4} of full-scale signal; this figure is most likely conservative because for the present purposes only drift over the duration of the test introduces error. The data were acquired at an approximate rate of one point every 2 s for the first 20 to 40 min following load application or removal, and thereafter at a rate of one point every 2 min. Each point was time stamped by the software after the multimeter completed a scan cycle.

Because L1501 is not of full-bridge design, the output might be expected to drift with thermal expansion of the material. Compensation elements are built into the gauge to reduce the drift. Gauge temperature was independently monitored with a thermocouple, but efforts toward further compensation by postprocessing were not fully successful. Figure 3 presents data collected over 55 h, with natural temperature variation of 1.5°C. In addition to a monotonic trend that could perhaps be attributed to anelasticity (the cell was under a 200-g load), the signal in Fig. 3b shows a cyclical pattern not captured by regression on temperature. (Inclusion of a quadratic temperature term did not improve the fit. It is speculated that an omitted variable, perhaps humidity or barometric pressure, might be responsible for the residual.) In contrast, such regression explains nightly changes of excitation voltage quite well; this result was not used, but is given for reference in Fig. 3c. Still, Fig. 3b provides an indication of the magnitude of thermal effects. The temperature coefficient obtained from it is $k_T = 6 \times 10^{-4}$ F.S./°C; a similar experiment at 15°C mean temperature yielded $k_T = 4 \times 10^{-4}$ F.S./°C. (Here and throughout the paper, F.S. denotes full-scale range of the relevant quantity, in this case the 1-mV/V full scale of gauge output.) Futek specifies $\pm 3.6 \times 10^{-4}$ F.S./°C zero drift and $\pm 3.6 \times 10^{-4}$/°C

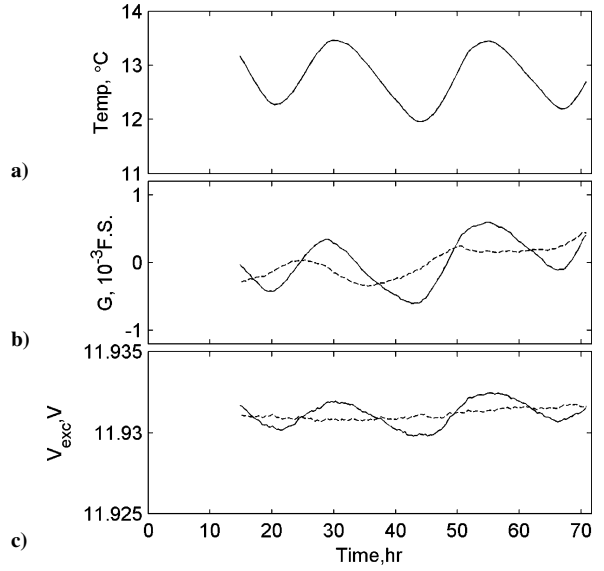

Fig. 3 Temperature regression of Futek L1501 bridge output: a) nightly temperature variation; b) bridge output (——) and regression residual (- - - -) as fraction of gauge full scale; and c) temperature regression of excitation voltage.

relative slope drift for L1501 at $15°C < T < 72°C$. Temperature excursion in most tests did not exceed 0.3°C and was too small to influence the results. Unless otherwise noted in the following, no temperature adjustment was applied to the data.

One measurement possibly compromised by the lack of temperature control was that of irreversible deformation under load. Sgobba et al.[11] loaded an Al-3.8% wt Cu sample to 0.1 of its elastic limit for 6 h and found that 2×10^{-4} fraction of the elastic strain became permanent. Permanent strain was recorded for all but one of the alloys studied, and in some appeared to be linear with the logarithm of time under stress.[13] Such irreversible effects as could be detected in the present work 24 h after a typical 20–40-min experiment were, given the uncertainty of the temperature correction employed, indistinguishable from zero. Consequently, plastic phenomena are not included in the analysis.

In addition to the apparatus in Fig. 2a, data were collected from the Twin Rotor Hover Performance (TRHP) test stand (Fig. 2b). The TRHP is similarly designed for microrotorcraft experiments, but differs in the arrangement of load-sensing elements. Two microrotors, of which only one is shown in Fig. 2b, are each supported on a 0.75-in. (19-mm) o.d. hollow aluminum beam and can be driven by a shaft passing through it. On the outside of each beam, two full-bridge strain gauges (Vishay Micro-Measurements EA-13-250PD-350) are

bonded with a strain-gauge adhesive (Vishay M-Bond AE-10). The full-scale load for TRHP is defined as 3.417 lbf (1.550 kgf) at the rotor, estimated to produce outer fiber stresses of 3.0 ksi (21 MPa) and 2.2 ksi (15 MPa) respectively under the rear and front gauges. These stresses equal 14% and 11% of nominal yield strength for general purpose aluminum and cause 3×10^{-3} and 2.2×10^{-3} strains. (The actual type of aluminum used is not known.) A signal conditioner provided both a nominal 10-V excitation for the bridges and 1000x preamplification; full-scale signal at its output was 4.6 V for front gauges and 6.25 V for rear gauges. Stability of the preamplifier, for which no specification is available, is not expected to be as good as that of the HP34970A; consequently, overnight experiments were not attempted.

III. Results

A. Estimation of Step Response

As noted earlier, the linear superposition principle, expressed in Eq. (1) for strain of the spring element, will herein be applied directly to bridge output, without discriminating the contributions of the spring, the gauge, and the adhesive. The roles played by these individual mechanisms are briefly discussed in Sec. IV; however, to the practical purpose of compensating anelastic error only the aggregate linearity is material.

Furthermore, it is clear that the output $G(t)$ depends not on time t as such, but on the history of stress $\sigma(t)$ prior to time t. The dependency can be broken up, nonuniquely, into a term dependent on the entire history and one reacting only to current stress,

$$G(\{\sigma(\tau)|\tau \le t\}) = G_E(\sigma(t)) + G_A(\{\sigma(\tau)|\tau \le t\}) \qquad (7)$$

It is sufficient to assume that linearity holds just for the second term in Eq. (7). In this way, sensors with slightly nonlinear characteristic $G_E(\sigma)$ can be considered, so long as their anelastic error obeys the superposition principle. Equation (7) is therefore restated as

$$G(t) = G_E(\sigma) + G_A(t) = G_E(\sigma) + \int_0^\infty u_A(\tau) M \dot{\sigma}(t-\tau)\, \mathrm{d}\tau \quad (8)$$

where the constant M, equal to the nominal sensitivity $\Delta G_E/\Delta\sigma$, is introduced for normalization. As defined in Eq. (8), the anelastic step response function $u_A(t)$ is dimensionless and, except perhaps at very small t, $|u_A(t)| \ll 1$. In the specific case of step load,

$$\sigma(t) = \begin{cases} 0, t < 0 \\ \sigma_0, t \ge 0 \end{cases} \Rightarrow G(t) = \begin{cases} G_E(0), t < 0 \\ G_E(\sigma_0) + M\sigma_0 u_A(t),\ t \ge 0 \end{cases} \qquad (9)$$

Measured time histories of strain under rising and falling step loads are presented in Fig. 4, along with curve fits by exponential and logarithmic functions. The exponential relationship, Eq. (3a), served as the starting point in Ref. 1; exponential series were also used extensively in Ref. 4. The logarithmic model is wholly empirical, but its accord with the data is superior. Especially remarkable is the model's ability to predict outside the 1000-s interval on which both curves were estimated. (Some of the difficulties encountered in Ref. 4 can perhaps be attributed to the unjustified extrapolation of the fitted exponential form.) Linear correction for temperature ($k_T = 4 \times 10^{-4}$ F.S./°C) helped improve the fit at $t = 3 \times 10^3$–6×10^3 s in Fig. 4a and $t = 7 \times 10^3$–2×10^4 s in Fig. 4b, but was not effective at later times. It appears most likely that the model fails earlier in Fig. 4a because of greater thermal or humidity effects not accounted for. The end portions of the data in Figs. 4a and 4b are also affected by the relaxation of prior loads. In each case, constant stress conditions were maintained for 24 h (8.6×10^4 s) immediately preceding the experiment. However, as the duration of the experiment itself approaches 24 h, anelastic aftereffects of even earlier events become significant in comparison to those of the more recent ones.

For formal identification of the step response, recast Eq. (9) in the form

$$\frac{G(t) - G_E(\sigma_0)}{G_E(\sigma_0) - G_E(0)} = \frac{M\sigma_0}{G_E(\sigma_0) - G_E(0)} u_A(t), \qquad t \ge 0 \quad (10)$$

A 1% inaccuracy in the factor $M\sigma_0/[G_E(\sigma_0) - G_E(0)]$ on the right-hand side of Eq. (10) implies only 1% inaccuracy in u_A and G_A. It is therefore acceptable to replace this factor with unity, neglecting any small nonlinearity of $G_E(\sigma)$. A similar simplification on the left-hand side would be ill advised. The denominator $[G_E(\sigma_0) - G_E(0)]$ is still well approximated from measured values of $G(t)$ before and after the load step, but the numerator is impacted decisively by even a small uncertainty of $G_E(\sigma_0)$. A constant offset term was added to the functional model for u_A to absorb the error. The offset, as Eq. (7) makes clear, can be arbitrarily redistributed between G_E and G_A.

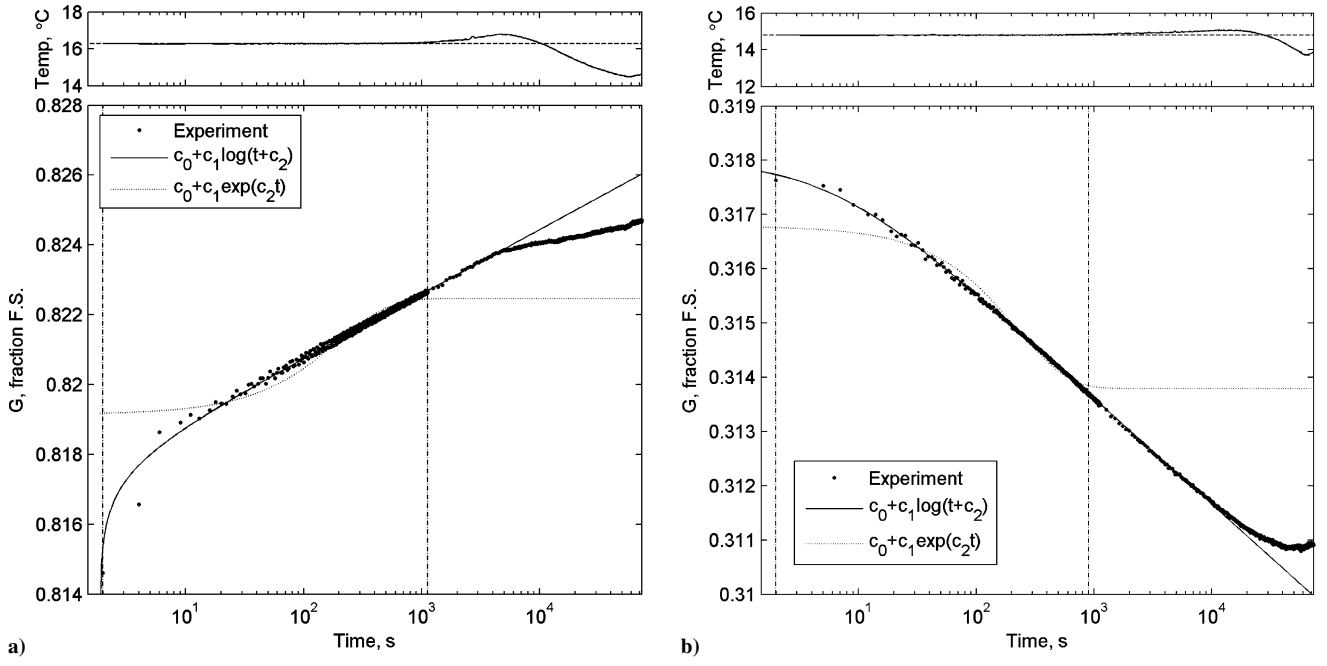

Fig. 4 Step response of bridge output to a) rising and b) falling stress in Futek L1501 load cell, curve fit by logarithmic and exponential functional forms. Vertical markers indicate the interval used for parameter estimation. Upper panels show variation of ambient temperature.

Table 1 Estimated parameters of the logarithmic step response model

	Data used for curve fit				
Load step	Duration, s	Temp. range, °C	No. points	c_1	c_2, s
$0 \rightarrow 100$ g	1145	15.5–15.6	491	0.001704	−2.8
$0 \rightarrow 100$ g	2311	16.2–16.3	996	0.001560	0.0
$0 \rightarrow 50$ g	2317	15.6–15.7	996	0.001599	1.4
$0 \rightarrow 200$ g	1121	16.3–16.4	489	0.001575	−1.9
100 g $\rightarrow 0$	2294	13.0–13.2	979	0.001668	2.7
200 g $\rightarrow 0$	902	14.8–14.9	391	0.001652	5.5

The ambiguity was resolved by requiring $u_A(1200\text{ s}) = 0$. The step response is consequently expressed as

$$u_A(t) = c_1 \log\left(\frac{t + c_2}{1200\text{ s} + c_2}\right), \qquad t \geq 0 \tag{11}$$

with two free parameters c_1, c_2 to be determined.

Curve fit results from six separate experiments are summarized in Table 1. The mean scale factor $c_1 = 0.00163 \pm 4\%$, a remarkable stability for a curve-fit estimate. The time offset c_2 is less certain and is in fact indistinguishable from zero. [Performance of the logarithmic model, Eq. (11), degrades only slightly with c_2 constrained to zero: relative standard deviation of c_1 rises from 4% to 6%.] This parameter is largely driven by the first few data points after loading, unreliable as a result of transients and the manual application of the load. Transients also prevented Sgobba et al.[13] from capturing the first 10 s of step response data. The validity of Eq. (11) at small t thus remains an open question for lack of good quality empirical observations.

In the sequel, the step response $u_A(t)$ is represented by Eq. (11) with coefficients c_1, c_2 obtained by joint regression of all six experiments listed in Table 1. (Each data set was first regressed individually to obtain fit coefficients $c_1^{(i)}$, $c_2^{(i)}$, $i = 1, 2, \ldots, 6$. The joint estimate used the mean value $\overline{c}_1 = 0.00163$ of $c_1^{(i)}$. The second parameter $\overline{c}_2 = 1.2$ s was found from six additional regressions in which c_1 was constrained to $\overline{c}_i$.) This form of $u_A(t)$ is utilized to compute and compensate anelastic error of the Futek L1501. Based on the foregoing, good results are anticipated starting at $t \sim 10$ s and through at least $t \sim 10^4$ s from the moment of load application or removal, a sufficient time horizon for typical scenarios of load cells' calibration and use. It is to be noted that the logarithmic law, Eq. (11), here only functions to approximate $u_A(t)$ in Eq. (8). A suitably chosen polynomial or other interpolation could serve equally well on the time interval where $u_A(t)$ has been dependably measured.

B. Compensation of Anelastic Error

Although Eq. (8) can be used directly when the stress σ is known, such as in calibration experiments, its application in other cases is simplified by eliminating σ. To this end, let $\sigma_E(G)$ be the inverse of the (nearly linear) memory-less part of the strain response $G_E(\sigma)$, so that from Eq. (7), $\sigma(t) = \sigma_E(G - G_A)$. Substituted into Eq. (8), this yields

$$G_A(t) = \int_0^\infty u_A(\tau) M \sigma_E'(G - G_A)\dot{G}(t - \tau)\,\mathrm{d}\tau - \int_0^\infty u_A(\tau) M \sigma_E'(G - G_A)\dot{G}_A(t - \tau)\,\mathrm{d}\tau \tag{12}$$

Because uncertainty in $M\sigma_E'(G - G_A)$ causes only proportional degree of uncertainty in G_A, the former can be approximately set to unity, neglecting the nonlinearity of σ_E. Further, the second integral in Eq. (12) involves a small quantity G_A and can be dropped under most circumstances, so that

$$G_A(t) \approx \int_0^\infty u_A(\tau)\dot{G}(t - \tau)\,\mathrm{d}\tau = \int_0^\infty c_1 \log\left(\frac{\tau + c_2}{1200\text{ s} + c_2}\right)\dot{G}(t - \tau)\,\mathrm{d}\tau \tag{13}$$

Equation (13) simply reflects the intuition that G_A can be estimated using an approximate value of stress $M^{-1}G(t)$ in Eq. (8) instead of the exact value $\sigma(t)$. The intuition is sustained so long as (and to the extent that) the output step response rises quickly to reach its near-flat anelastic portion.

The fitting parameters c_1, c_2 from Eq. (11) and Table 1 are all that is needed to evaluate and compensate the anelastic error in any bridge output profile $G(t)$ by means of Eq. (13). Figures 5 and 6 offer examples. In Fig. 5, each of the top frames portrays the load history of a particular experiment. Two lower frames depict raw and compensated error:

$$e_{\text{raw}} = G(t) - G_E(\sigma)$$

$$e_{\text{comp}} = G(t) - G_E(\sigma) - \int_{t_0}^\infty u_A(\tau)\dot{G}(t - \tau)\,\mathrm{d}\tau \tag{14}$$

where for simplicity the elastic response $G_E(\sigma)$ is represented by a linear form $G_E(\sigma) = M\sigma$. Failures of the model of $G_E(\sigma)$ and failures of the model of $u_A(\tau)$ both contribute to the residual e_{comp}; however, the former cause e_{comp} to vary with stress σ, whereas the latter cause it to vary with time at constant stress. Defects seen in Fig. 5 are almost entirely of the first kind. An rms noise floor of 2×10^{-5} F.S. with data points taken every 2 s, as in Fig. 5a, was typical; greater noise in Fig. 5b (which, however, does not obscure the trend) is almost certainly caused by the rocking motion of the weight pan during some of the load periods. (Reference 14 reports that a 10^{-4} F.S. noise floor target could not be met, possibly because of commercial aircraft operating nearby. No such difficulties were experienced in the present work.)

The extent to which time-varying anelastic error has been explained might be quantified as follows. Suppose that Fig. 5a represents a record of manual calibration in which four loads were applied, and suppose further that the calibration data point could be taken with equal probability at any time while the load was in place, excluding the first and last 15 s. Insofar as the reading varies under constant load, uncertainty is introduced into the data. In the case of Fig. 5a, accounting for anelastic behavior reduces this uncertainty by 99.5%. (This figure of merit is imperfect, however: random noise and range limitation from shorter load steps deflate it to 57% in Fig. 5b, even though anelasticity is modeled no worse there than in Fig. 5a.)

Figure 5a also demonstrates that, as a consequence of linear superposition, apparent relaxation rates differ from one load period to the next. If each of the four curve segments in $e_{\text{raw}}(t)$ were individually fitted with an exponential decay function, time constants of 583, 589, 240, and 478 s, respectively, would be found. [A similar outcome is likely if the entire curve were jointly fitted by a sum of four exponential functions. This is because the exponential tends to go flat immediately outside the estimation interval (compare Fig. 4).] It is to be emphasized that the time constants depend here not on stress or stress rate [in which Eq. (8) is linear], but on stress history. Description of anelastic phenomena in terms of relaxation times, often encountered in the literature, is therefore quite ambiguous.

The effectiveness of Eq. (13) is further evident in Fig. 6, where the calibration experiment from Fig. 5b appears again, along with a similar calibration carried out the next day. In Fig. 6, each load point is represented by its mean value, and uncertainties are indicated by error bars. Regression of the two raw data sets on applied loads yields

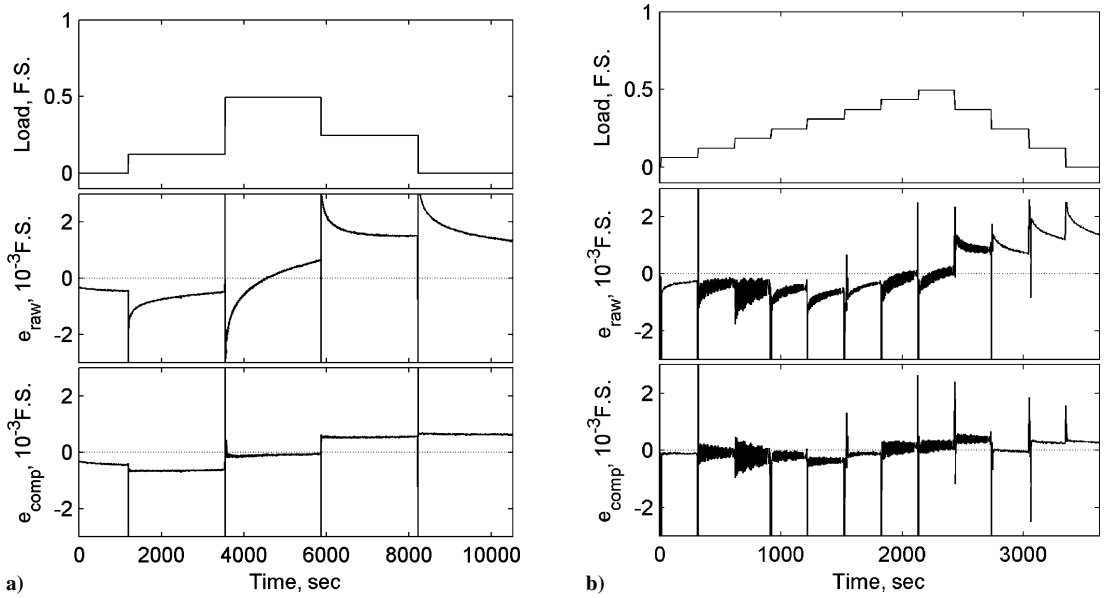

Fig. 5 Compensation of anelastic error: top frames, load history; middle frames, raw error; and bottom frames, residual after compensation.

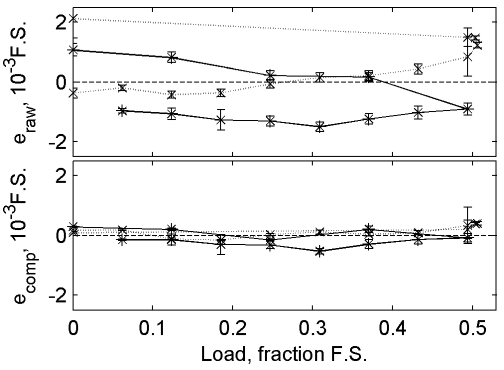

Fig. 6 Compensation of anelastic error in two independent calibrations (—— and - - - -) of Futek L1501. Residual calibration error without (top) and with (bottom) compensation of anelastic behavior.

two estimates of sensitivity $M = \Delta G_E / \Delta\sigma$ that differ by 0.4%, with rms residuals of 0.08–0.09%. In contrast, the two sensitivities differ by only 0.1% and rms residuals drop to 0.02% when the data are corrected for anelastic effects.

To confirm that the phenomena under investigation are not unique to Futek L1501, one 40-min step loading/unloading experiment was performed on each of the four bending beam elements of the TRHP stand. The results obtained were quite similar. Stress, raw, and compensated error profiles from the four tests are reproduced in Fig. 7. The part of each data set with load applied was used to estimate the element's step response and was backcomputed. However, cross-computed compensation for the later parts with load removed is seen to be equally effective. The relatively large difference between initial and final readings from gauges RF, RB is thought to be caused by friction in the plastic and neoprene flexible couplers that, together with the drive shaft, make up an unwanted load path (Fig. 2b). Model parameters $c_1^{(i)}$ for the four elements [compare Eq. (11)] were estimated at 0.00125, 0.00103, 0.00153, and 0.00132. Because only one data set is available for each element, it is not known whether the variation in c_1 is spurious or substantive.

Although the examples offered in this section all pertain to calibration, test data can and should be compensated for anelastic error in a similar manner. Because the superposition principle, Eq. (8), holds, the time-averaged error behaves as if stimulated by the time-averaged stress. High-frequency vibration experienced during the test therefore need not be taken into account, and the uncertainty of $u_A(t)$ for small t causes no difficulty. To the extent that a test proceeds through its sequence of load conditions slower than does calibration, the impact of anelasticity on test data might be less significant.

IV. Discussion

A. Consequences of Anelastic Behavior

To aid understanding of the impact anelastic behavior, if not accounted for, can have on measurement results, this subsection offers two synthetic examples. The first of these, appearing in Fig. 8, reflects a scenario typical of single-gauge manual calibration of a wind-tunnel balance. Altogether 15 load points are taken, with a 60-s setup time and 30-s measurement time for each point. For the purposes of simulation, it is assumed that the gauge exhibits the same amount of anelasticity as Futek L1501 and is ideally linear otherwise. The error history is shown in the lower frame of Fig. 8a, the markers indicating times close to the end of each load period when the bridge output is recorded. The recorded data comprise the calibration database, subsequently to be reduced by global regression. True error of the acquired data points can be seen in Fig. 8b. Despite the symmetric appearance of the load profile, bias is evident in Fig. 8b that will cause the regression to underestimate gauge sensitivity. The misestimate is greater the more rapidly the load schedule is traversed (Fig. 8c) and can reach 0.5%; yet the rms backcomputed residual, frequently used as a metric of calibration quality, gives no indication of the problem (Fig. 8d).

The curves in Figs. 8c and 8d stop at the 500-s point only because a 15-load manual calibration in less time seems impractical. Should the procedure be further expedited by taking fewer points or by using automatic equipment, even greater systematic error results. On the other hand, because of the logarithmic nature of the relationship, only marginal benefit is realized from slowing the action down (Fig. 8c). If accuracy is to be improved beyond 0.3%, proper accounting for the anelastic effect is essential.

The second example, Fig. 9, shows a time history typical of a TRHP experiment. A check load is applied, followed by a series of thrust measurements as the rotor collective pitch is gradually increased. A repeat pass is taken in the same direction to avoid hysteresis in the setting of collective pitch. It is seen in Fig. 9 that the heavy loads at the end of the first pass cause an error early in the second pass that exceeds 0.4% of full scale and is a much greater fraction of the small thrust loads upon which it is superimposed. The hazard of taking a zero point soon after the removal of a check load is also apparent.

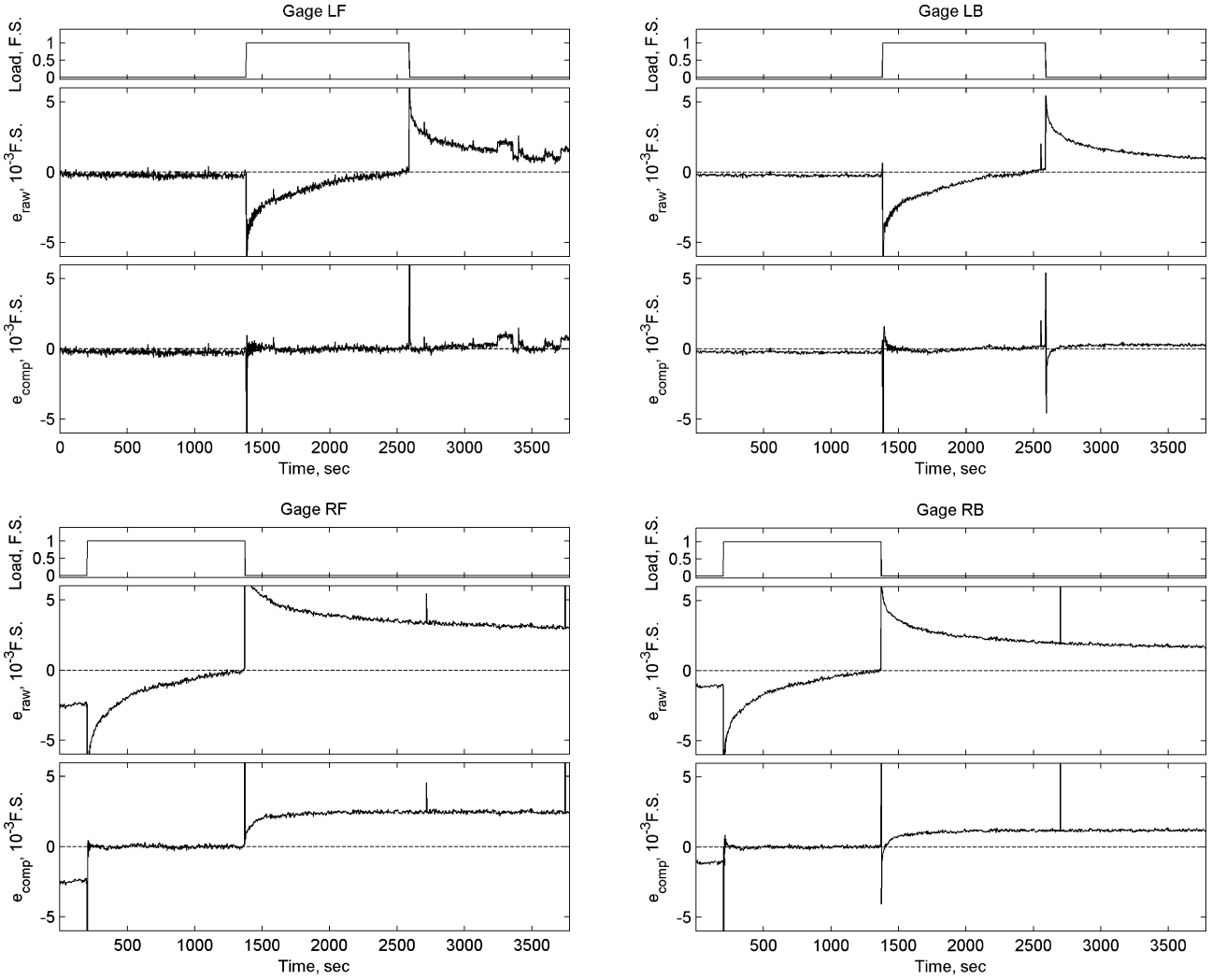

Fig. 7 Compensation of anelastic error in TRHP gauges: top frames, load history; middle frames, raw error; and bottom frames, residual after compensation.

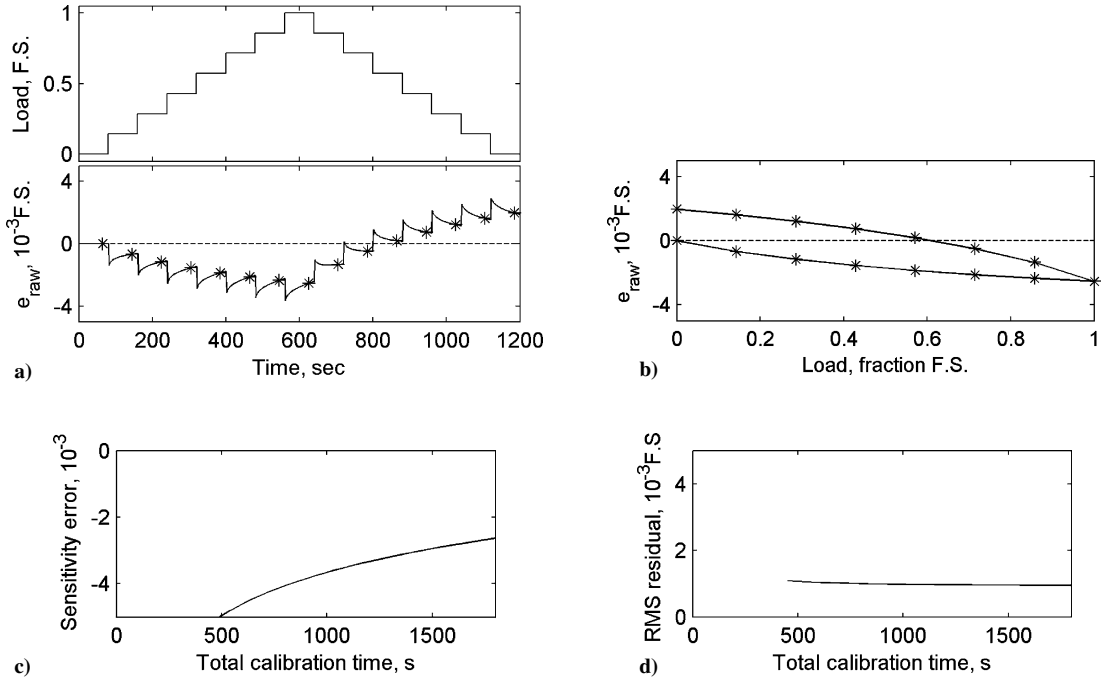

Fig. 8 Simulated calibration of a perfectly linear but anelastic gauge: a) calibration time history; b) true error of calibration data; c) bias of sensitivity estimate as function of calibration time; and d) backcomputed rms residual error.

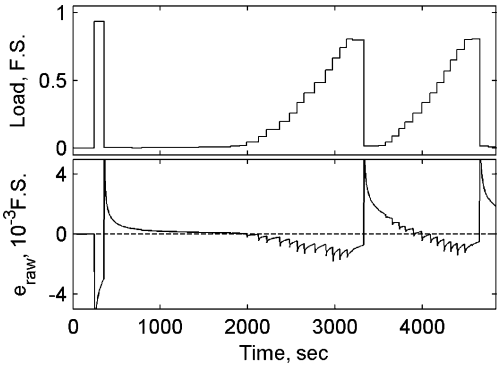

Fig. 9 Load history and estimated error in a typical TRHP experiment.

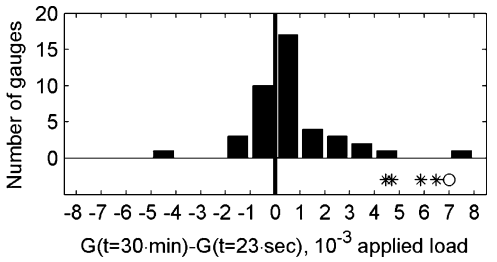

Fig. 10 Net drift under load in 42 gauges of seven six-component wind-tunnel balances. Based on data from Ref. 3. Markers indicate for comparison the performance of Futek L1501 (○) and the four gauges in the TRHP (∗).

B. Anelastic Behavior in Wind-Tunnel Balances

Internal wind-tunnel balances, because of their extensive use, are of particular interest to the aerodynamics community. Being a fundamental property of crystalline solids, anelasticity is expected to manifest itself in all devices, including balances, to some degree. However, its significance may be reduced when premium materials are used, or when other types of error are brought into dominance by the instrument's complexity, or both. Alternatively, that same complexity may compel the instrument's designer to accept engineering tradeoffs at the expense of anelastic performance.

Despite the practical importance of wind-tunnel balances, few direct measurements of their anelastic properties have been reported. A recent work of Cahill et al.[3] appears to be the only one thus far to include such data. The study compared, as one factor among several, anelastic characteristics of new balances from seven vendors. For each balance, and within the balance for each of the six gauges, the net change of output from approximately the 23rd second to the 30th minute under steady load was recorded. All measurements were made in the Allied Aerospace ABCS machine with reference to the machine's own load cells. (The ABCS machine applies a load rapidly and stabilizes in 5–10 s depending on the magnitude of the load change. The first measurement began immediately upon stabilization and consisted of five samples spanning a 30-s period. The midpoint of the measurement interval thus falls close to the 23rd second.) The anelasticity of the ABCS cells themselves was found to be negligible in previous work,[14] although some doubts remain. [The ABCS cells are not routinely calibrated for anelasticity; the cells utilized in Ref. 3 might not have been the ones investigated in Ref. 14. In Ref. 14 itself, anelasticity of the load cell was not thought to exceed 10^{-4} of applied load; however, only 24 data points were taken, outliers had to be manually removed, and the exponential fit, Eq. (3b), was used in analysis.]

Figure 10 summarizes the results from Ref. 3. (The sign of output change in Fig. 10 is reversed relative to Ref. 3, in which later gauge readings were subtracted from earlier readings.) Its evidence suggests that most wind-tunnel balances, or at least most balances of recent manufacture, are less anelastic than the inexpensive load cells investigated in Sec. III. Still, the error in one of the gauges exceeds that of Futek L1501 and in five others comes within a factor 3.3 of it, enough to render a 20-min manual calibration similar to that in Fig. 8 over 0.1% inaccurate. Evaluation of anelastic performance of each balance before use therefore seems advisable.

The recommended balance calibration procedure defined by AIAA in Ref. 15 does not collect the data necessary for such an evaluation. A calibration database, as described in Ref. 15, is a record of applied load vectors in one-to-one correspondence with bridge output vectors. A mathematical model, consisting of first- and second-order terms, first-order interactions, and sometimes absolute value and/or third-order terms, is fitted to the database by global least-squares regression. The database is not sufficient to distinguish model error (i.e., the model's inability to capture high-order nonlinear behavior of the balance) from random measurement error, much less tease out the systematic measurement error of which anelastic error may be one part. This weakness is recognized in Ref. 15 itself: its Sec. 3.5, "Emerging Technologies," proposes the use of experimental randomization to identify systematic errors generally, and the capture of step response curves to assess the magnitude of anelasticity in particular. As of yet, however, neither technique has been widely adopted.

C. Interpretation of Anelastic Behavior in Force Sensors

As already pointed out, the object of the present investigation is the ultimate electrical response of the load cell. The approach used rests entirely on the empirical linearity of time-varying output error with applied stress; assumptions with respect to the origins of the error are not essential. However, a few brief comments are in order.

Creep in the stress-bearing spring material, the strain gauge, and the adhesive bond between the gauge and the spring all influence bridge output. The creep tendency of a strain gauge depends in part on the pattern of the resistive film and can be either positive (in the direction of stress) or negative. Vendors offer gauges in a range of creep grades, designed to compensate, within certain limits, for the aberrations of the spring material.[16] (The same adhesive is recommended in all cases, however, suggesting that the contribution of adhesive creep is either small or hightly consistent.)

Anelastic responses plotted in Fig. 11 are most likely the consequence of such compensation. Figure 11 offers a glimpse into the large amount of data collected by the National Institute of Standards and Technology from transducers submitted there for certification between 1992 and 1996 (Ref. 2). The curves exhibit both upward and downward trends and sometimes sharp reversals within 10 min of loading. It is not clear from Ref. 2 whether any of the patterns are encountered more often than others. In some cases, as in Figs. 11c and 11d, the same load cell responds in a qualitatively different manner at ambient 20°C (68°F) than it does at 40°C (104°F). The variety and volatility of features suggest that Fig. 11 may be revealing the net result of mutual near cancellation of multiple mechanisms, each having its own timescale and thermal dependency. This conjecture is further supported by the relatively low magnitude of the response. [The difference between creep (loading) and recovery (unloading) curves in Fig. 11 must be partly, perhaps mostly, due to the fact that the latter immediately followed the former. No attempt was made in Ref. 2 to estimate a proper linear model by inverting the superposition relation, Eq. (1).]

In contrast, given the smooth form of the Futek L1501 creep curve in Fig. 4, with no obvious discontinuities or inflections between $t = 10$ and 10^4 s, it seems plausible that the same mechanism dominates throughout. Moreover, it may be speculated that the dominant contribution is attributable to the strain gauge. This is because 1) the signal trends up over time, contrary to expectation for adhesive effects, and 2) the step responses obtained appear to be in disagreement with results previously reported for bulk metals. On the second point, because creep characteristics change with temperature, room-temperature experiments of Sgobba et al.[11–13] provide the only data available for comparison. Sgobba et al. measured flexural deformation of thin copper and aluminum strips under constant stress. The size of the anelastic effect, as quantified by the amount of strain acquired in 30 min after loading, depended significantly on the composition of the alloy and on sample preparation, being in some cases

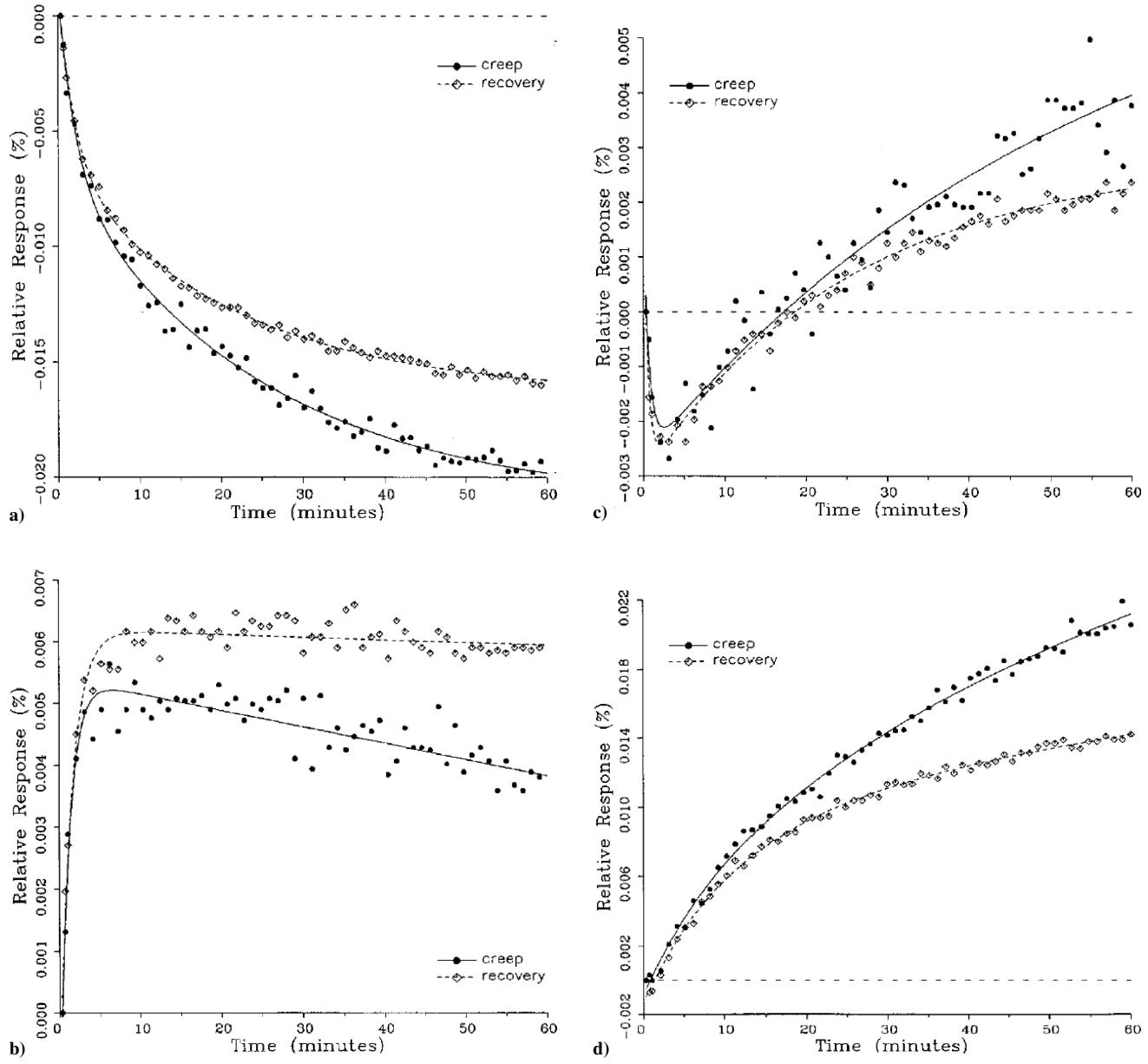

Fig. 11 Step response curves of some of the load cells submitted to NIST for certification. Reproduced from Ref. 2.

(Al7075:T651; Ref. 13) similar to that obtained herein for load cells, whereas in other cases (Cu-2%Be; Ref. 12) two orders of magnitude below it. In every instance, however, the growth of strain with time roughly followed a power law, $\varepsilon \sim t^n$, $n \approx 0.5$. Logarithmic relationship was never observed. (Anelastic creep thus differs from plastic (permanent) creep, for which logarithmic growth at low temperatures is the rule.[6]) The power law is also in better accord with Lubahn's data on steel at 800°F (476°C) (Ref. 4).

This analysis is encouraging. For, if the present results can be interpreted as a demonstration that linear superposition holds for the creep of strain gauges, and because it likewise holds for the anelastic response of metals,[4] one can be hopeful that the methodology proposed herein will prove applicable to a broad variety of force measuring devices. There is also hope that the thermal sensitivity evident in Fig. 11 is characteristic only of well-tuned transducers in which creep contributions of components nearly cancel one another; if so, devices that exhibit greater anelastic error (and which are consequently of greater interest) would not require calibration at the operating temperature. More study is of course required before either of the preceding claims can be made with any confidence.

V. Conclusions

An empirical model of anelastic behavior in force and moment sensors has been presented. The high degree of linearity exhibited by anelastic phenomena permits a step response function captured during calibration to be used for prediction and compensation of the error in the remainder of the calibration data and in the actual test. In the two types of bending beam load cells investigated, the model explains all or nearly all of the time-dependent output change under constant load.

The anelastic step response is found to be well approximated by a logarithmic function of time, with only two free parameters, at least between $t \sim 10$ and 10^4 s (2 h 45 min) from the moment of load application or removal. The proposed logarithmic form substantially differs from, and performs better than, exponential decay functions used previously, particularly in predicting data outside the sample on which it had been estimated. Time constants obtained for anelastic relaxation by exponential fit, frequently reported in the literature, are shown to be inconsistent and depend on stress history.

Manual loading and lack of temperature control prevented accurate acquisition of the step response prior to $t \sim 10$ and past $t \sim 10^4$ s

from the moment of load application. Because anelastic creep slows over time, and because neither calibrations nor tests tend to run longer than 3 h without major changes in load conditions, the 10^4-s time horizon of the step response is adequate for most applications. Nor does the uncertainty at $t < 10$ s present a problem unless high-frequency transients must be captured with sub-1% accuracy. Should the need arise, however, appropriate experimental techniques can be used to measure the step response on any relevant timescale.

Anelastic behavior is most pronounced when the stress changes fast and by a large amount. Consequently, zero points taken soon after removing a load, and small loads measured in the aftermath of large loads, are particularly vulnerable. A calibration in which the load is ramped up and then down over a 20-min period might be over 0.3% inaccurate. The error will reproduce whenever the same load program is executed; worse still, most of the error is absorbed into the linear term of the mathematical model and is not detected by backcomputation. Design of experiment methodologies, which could reveal this and other systematic problems, are rarely followed.

The present work is limited, most importantly, in the number and kinds of load cells investigated. Only one quarter-bridge and one batch of full-bridge elements were studied, with most attention given to the former. Effects, if any, of stress reversal were not examined, and none of the elements exhibited creep in the direction opposite stress, as has been observed by other researchers in some wind-tunnel balances. No data were taken at elevated temperatures [up to 50°C (122°F)] characteristic of many wind-tunnel operations.

Because no interferometric or other independent measurement of strain was available, the contributions of material anelasticity, adhesive creep, and defects of the strain gauges themselves could not be separately identified. Simultaneous monitoring of mechanical deflection and bridge output would do much to clarify the phenomena taking place at the interface of strain gauge and spring material.

These limitations are mitigated, however, by the ease with which the result can be used in practice. A set of calibration weights and software capable of continuous data acquisition over a few hours is all that is needed to capture the step response, estimate model parameters, apply the model, and evaluate its effectiveness for a particular force-sensing device. It is hoped that this procedure will become routine whenever sub-1% measurement uncertainty is sought. In the many—perhaps most—cases when the time-dependent error (whether or not of logarithmic form) obeys linear superposition, the quality of both test and calibration data can then be significantly improved by simple postprocessing. In all cases, the exercise will help assess the magnitude of creep in the instrument. This is of particular importance for wind-tunnel strain-gauge balances because so little empirical data on the anelastic behavior of these widely used instruments are currently available.

Acknowledgments

The author thanks Jeffrey L. Johnson, Benton Lau, and the NASA Ames Aeromechanics Branch for the use of microrotor test stands with which the data in this work were collected; William D. Nix for help in interpreting anelastic behavior of metals; Johannes van Aken, Jeffrey L. Johnson, Frank Steinle, and Dennis Booth for information regarding the calibration of wind-tunnel balances; and Gene Ruzicka, Wayne Johnson, Thomas Maier, William Warmbrodt, Gloria Yamauchi, and all staff of the NASA Ames Aeromechanics Branch for their support and helpful suggestions.

References

[1]Steinle, F. W., "Modeling of Anelastic Effects in Calibration of a Six-Component Wind Tunnel Balance," AIAA Paper 2000-0150, Jan. 2000.

[2]Bartel, T. W., and Yaniv, S. L., "Creep and Creep Recovery Response of Load Cells Tested According to U.S. and International Evaluation Procedures," *Journal of Research of the National Institute of Standards and Technology,* Vol. 102, No. 3, 1997, pp. 349–362.

[3]Cahill, D., Steinle, F., and Richardson, S., "Evaluation of Wind Tunnel Internal Force Balances from Seven Vendors," AIAA Paper 2004-1292, Jan. 2004.

[4]Lubahn, J. D., "The Role of Anelasticity in Creep, Tension, and Relaxation Behavior," *Transactions of the American Society for Metals,* Vol. 45, 1953, pp. 787–838.

[5]Oehlert, A., and Atrens, A., "Room Temperature Creep of High Strength Steels," *Acta Metallica and Materialia,* Vol. 42, No. 5, 1994, pp. 1493–1508.

[6]Nabarro, F. R. N., and deVilliers, H. L., *The Physics of Creep*, Taylor and Francis, London, 1995, Chap. 3.4.

[7]Zener, C., *Elasticity and Anelasticity of Metals*, Univ. of Chicago Press, Chicago, 1948.

[8]Ke, T. S., "Experimental Evidence of the Viscous Behavior of Grain Boundaries in Metals," *Physical Review,* Vol. 71, No. 8, 1947, pp. 533–546.

[9]Ke, T. S., "Fifty-Year Study of Grain-Boundary Relaxation," *Metallurgical and Materials Transactions A,* Vol. 30A, No. 9, 1999, pp. 2267–2295.

[10]Golovin, I. S., Neuhauser, H., Riviere, A., and Strahl, A., "Anelasticity of Fe-Al Alloys, Revisited," *Intermetallics,* Vol. 12, No. 2, 2004, pp. 125–150.

[11]Sgobba, S., Kunzi, H. U., and Ilschner, B., "Measurement and Analytical Interpretation of the Anelastic Behavior of Al Alloys," *Zeitschrift fur Metallkunde,* Vol. 83, No. 8, 1992, pp. 572–576.

[12]Sgobba, S., Voegeli, M., Kunzi, H. U., and Ilschner, B., "A Study of Room Temperature Anelastic Creep of Cu–Be," *Journal de Physique IV*, Vol. 6, No. 8, 1996, pp. 251–254.

[13]Sgobba, S., Kunzi, H. U., and Ilschner, B., "The Influence of Thermal and Surface Threatments on the Anelastic Creep of Al-Zn and Al-Cu Alloys," *Acta Metallica and Materialia,* Vol. 43, No. 3, 1995, pp. 1171–1181.

[14]Steinle, F. W., Booth, D., and Rhew, R., "Determination of Anelasic-Induced Error in Wind Tunnel Test Force and Moment Measurements," AIAA Paper 99-0682, Jan. 1999.

[15]"Recommended Practice: Calibration and Use of Internal Strain Gage Balances with Application to Wind Tunnel Testing/Sponsored by American Institute of Aeronautics and Astronautics," AIAA, Rept. R-091-2003, Reston, VA, 2003.

[16]"BLH: Transducer Gages and Accessories, Catalog No. 306," Vishay Measurements Group GmbH, Heilbrun, Germany, 2001, URL: http://www.blh.de/pdftg/cat_tg.htm [cited 23 Aug. 2004].

A. Palazotto
Associate Editor